



# CHALMERS

## Chalmers Publication Library

### **Deterministic assembly of linear gold nanorod chains as a platform for nanoscale applications**

This document has been downloaded from Chalmers Publication Library (CPL). It is the author's version of a work that was accepted for publication in:

**Nanoscale (ISSN: 2040-3364)**

Citation for the published paper:

Rey, A. ; Billardon, G. ; Lörtscher, E. (2013) "Deterministic assembly of linear gold nanorod chains as a platform for nanoscale applications". *Nanoscale*

<http://dx.doi.org/10.1039/C3NR02358C>

Downloaded from: <http://publications.lib.chalmers.se/publication/180428>

Notice: Changes introduced as a result of publishing processes such as copy-editing and formatting may not be reflected in this document. For a definitive version of this work, please refer to the published source. Please note that access to the published version might require a subscription.

Chalmers Publication Library (CPL) offers the possibility of retrieving research publications produced at Chalmers University of Technology. It covers all types of publications: articles, dissertations, licentiate theses, masters theses, conference papers, reports etc. Since 2006 it is the official tool for Chalmers official publication statistics. To ensure that Chalmers research results are disseminated as widely as possible, an Open Access Policy has been adopted. The CPL service is administrated and maintained by Chalmers Library.

(article starts on next page)

## Deterministic assembly of linear gold nanorod chains as a platform for nanoscale applications†

Cite this: DOI: 10.1039/c3nr02358c

Antje Rey,<sup>\*ab</sup> Guillaume Billardon,<sup>a</sup> Emanuel Lörtscher,<sup>a</sup> Kasper Moth-Poulsen,<sup>c</sup> Nicolai Stuhr-Hansen,<sup>d</sup> Heiko Wolf,<sup>a</sup> Thomas Bjørnholm,<sup>e</sup> Andreas Stemmer<sup>b</sup> and Heike Riel<sup>a</sup>

We demonstrate a method to assemble gold nanorods highly deterministically into a chain formation by means of directed capillary assembly. This way we achieved straight chains consisting of end-to-end aligned gold nanorods assembled in one specific direction with well-controlled gaps of ~6 nm between the individual constituents. We determined the conditions for optimum quality and yield of nanorod chain assembly by investigating the influence of template dimensions and assembly temperature. In addition, we transferred the gold nanorod chains from the assembly template onto a Si/SiO<sub>2</sub> target substrate, thus establishing a platform for a variety of nanoscale electronic and optical applications ranging from molecular electronics to optical and plasmonic devices. As a first example, electrical measurements are performed on contacted gold nanorod chains before and after their immersion in a solution of thiol end-capped oligophenylenevinylene molecules showing an increase in the conductance by three orders of magnitude, indicating molecular-mediated transport.

Received 8th May 2013

Accepted 6th July 2013

DOI: 10.1039/c3nr02358c

[www.rsc.org/nanoscale](http://www.rsc.org/nanoscale)

### 1 Introduction

Inorganic nanoparticles with size dimensions and tunable properties barely achievable by conventional top-down fabrication techniques are very attractive bottom-up building blocks for nanoscale electronics<sup>1–10</sup> as well as for nano-optical applications.<sup>11–14</sup> These building blocks need to be integrated and connected to the existing architecture which requires the controlled placement and spacial arrangement of nanoparticles in an efficient way over large areas. However, achieving full control over the alignment and position of such nanoparticles remains challenging.<sup>15,16</sup> Recently, gold nanorods (Au NRs) in particular have attracted great interest owing to their elongated shape, which offers interesting physical properties for various applications ranging from electronic and optical devices to sensing and imaging or diagnostics.<sup>17–20</sup>

To render Au NRs feasible as a bottom-up platform for applications, various approaches have been investigated to

control their assembly in three-dimensional (3D), two-dimensional (2D), or one-dimensional (1D) nanostructures.<sup>21,22</sup> For example, by means of large-area 2D block copolymer templates, the assembly of Au NRs in curved lines has been achieved.<sup>23</sup> Furthermore, surface interactions based on chemical functionalization and surface patterning have been used to control the assembly of arrays of Au NRs.<sup>24</sup> Typically, to obtain tight chains of Au NRs, a pre-organization by chemically linking the Au NRs in the solution phase prior to deposition is employed.<sup>25–30</sup> These methods however provide limited control over the position, orientation and linearity of the Au NR chains. Hence so far the controlled and reproducible assembly of Au NRs in straight lines with sub-10 nm distance on a generic substrate has not been achieved.

Au NRs are highly suitable electrodes for molecular electronics as their crystalline structure and small diameter of typically 20–30 nm make it possible to contact only a small number of molecules at the tip interface. Also the fact that thiols, the best studied molecular anchor group, chemically bond to Au renders Au NRs attractive for such applications.<sup>31</sup> Using a seed-mediated approach, Jain *et al.* fabricated single nanogap junctions *in situ* between lithographically pre-patterned metal contacts and Au NRs.<sup>32</sup> However, deterministic control over the integration of Au NRs onto appropriate substrates and in devices remains a key challenge for exploiting their unique properties in technological applications.

A promising method for assembling the Au NRs is directed capillary self-assembly which employs pre-structured templates to achieve highly deterministic placement of the nanoparticles

<sup>a</sup>IBM Research – Zurich, Säumerstrasse 4, 8803 Rüschlikon, Switzerland. E-mail: rey@zurich.ibm.com; Tel: +41-44 724 8236

<sup>b</sup>Nanotechnology Group, ETH Zürich, Säumerstrasse 4, 8803 Rüschlikon, Switzerland

<sup>c</sup>Department of Chemical and Biological Engineering, Chalmers University of Technology, Kemivägen 4, 41296 Gothenburg, Sweden

<sup>d</sup>Department of Drug Design and Pharmacology, University of Copenhagen,

Universitetsparken 2, 2100 Copenhagen, Denmark

<sup>e</sup>Nano-Science Center & Department of Chemistry, University of Copenhagen, Universitetsparken 5, 2100 Copenhagen, Denmark

† Electronic supplementary information (ESI) available. See DOI: 10.1039/c3nr02358c

in two dimensions.<sup>33–35</sup> In this method, a droplet of a colloidal solution is moved in a controlled manner over a structured polymer template to assemble particles *via* the three-phase contact line of a receding meniscus. By using the polymer template as a stamp, the particles can then be transferred directly onto a target substrate, *e.g.*, an oxide-covered silicon substrate (Si/SiO<sub>2</sub>), for further processing or onto a substrate with pre-structured leads for direct electrical measurements. The directed capillary self-assembly method was initially described to enable the deposition of symmetrical polystyrene (PS) and Au nano-spheres in arrays as well as in lines.<sup>36,37</sup> Using this method, individual Au NR dimers<sup>38</sup> and single Au NRs<sup>39</sup> were assembled into linelets and ensembles of Au NRs<sup>40</sup> directed into trenches. However, because of the anisotropic shape of the Au NRs the precise control over their orientation and their relative positioning in respect to adjacent Au NRs remained unsatisfying.

In this work we demonstrate the highly deterministic assembly, transfer, and characterization of oriented and tightly positioned Au NRs aligned end-to-end with nanometer-sized distances resulting in straight linear Au NR chains, by directed capillary self-assembly. Furthermore, we examine the constitutive correlation between the template geometry and the selectivity and quality of the assembled Au NR chains. In addition, we developed a process to transfer the Au NR chains without distortion onto a Si/SiO<sub>2</sub> substrate. Finally, the Au NR chains fabricated by this method were contacted using electron beam lithography (EBL) and lift-off technique and were electrically characterized before and after functionalization with oligophenylenevinylene (OPV-5) molecules. The assembly process developed paves the road for the controlled fabrication of highly deterministic structures for various applications in the broad fields of nano-electronics, nano-optics, as well as nano-medicine and sensors.<sup>41,42</sup>

## 2 Results and discussion

### Assembly of highly deterministic Au NR chains

The assembly of Au NRs into pre-structured polydimethylsiloxane (PDMS) templates with high selectivity and high accuracy in terms of position and alignment strongly depends on the correlation between the size of the individual constituents of the nanoparticle colloid and the geometry of the assembly template. Therefore, the size distribution and shapes of the Au NRs influence the assembly process. The Au NRs used in this study possess an aspect ratio of  $\sim 3$  with a surface plasmon resonance (SPR) at  $\sim 730$  nm. They are stabilized in a cetyltrimethylammoniumbromide (CTAB) solution, which serves as a cationic surfactant and adsorbs on the Au NR surface in the form of a self-assembled bilayer bound through electrostatic interactions between the cationic head group and anionic sites on the Au surface.<sup>43</sup> Owing to the seed-mediated synthesis of the Au NRs, they are not homogeneous in all three dimensions. Diameter variations in particular are critical for accurate end-to-end alignment in template channels of a fixed width. Examination of the Au NR size distribution (see ESI, Fig. SI 1†) resulted in a mean value of 64 nm (variance  $\sigma^2 = 5$  nm) for the

length and of 24 nm ( $\sigma^2 = 4$  nm) for the diameter. The assembly templates were made from PDMS<sup>44</sup> by molding the polymer against a hydrogen silsesquioxane (HSQ) resist patterned silicon master wafer with various channel structures as shown schematically in Fig. 1. The resulting structures in the PDMS template after molding were channels designed to be 90  $\mu$ m in length and with widths ranging from 20 to 90 nm. The thickness of the HSQ structures defines the channel depths and was varied from  $40 \pm 3$  nm to  $60 \pm 3$  nm and  $80 \pm 3$  nm.

For the assembly experiments, a droplet ( $\sim 50$ – $60$   $\mu$ L) of the colloidal suspension of Au NRs is deposited over the entire assembly template. The droplet is then confined between the structured template and a fixed silicon slide, which pins the meniscus of the droplet close to the slide (Fig. 2a). By moving the structured template on a translational stage relative to the fixed silicon slide, the meniscus of the droplet is actively moved over the structured area of the template. In contrast to earlier capillary assembly experiments, here the stage is moved parallel to the axis of the channel structure as shown schematically in Fig. 2b. This results in the forefront of the meniscus aligning almost perpendicular to the axis of the channels (Fig. 2c). The dense accumulation of Au NRs at the meniscus directs them into the channels by capillary forces as shown schematically in Fig. 2a and b.<sup>36</sup> Owing to their anisotropic shape, the Au NRs align preferentially parallel to the forefront of the meniscus<sup>38</sup> and experience a strong capillary-induced angular momentum in the proximity of the trapping channels, which finally aligns them tightly into the channel structure (Fig. 2b). By this method, chains composed of a few tens of Au NRs can be assembled in the channels, resulting in chain lengths of up to several micrometers as indicated by the bright lines in Fig. 2c.

### Optimization of the assembly yield by tuning the template properties and the assembly parameters

The successful assembly of Au NRs into channels requires a stringent geometrical matching between the assembly template and Au NRs in particular regarding the channel width and depth. First we investigated the influence of the channel depth in the range of  $40 \pm 3$  nm,  $60 \pm 3$  nm, and  $80 \pm 3$  nm on the assembly result. Whereas the Au NRs were not deposited into the channels if the channels had a depth of 40 nm, the assembly

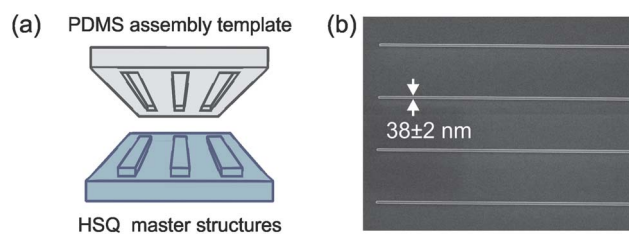


**Fig. 1** Template fabrication: (a) the nanoscale channels in the PDMS assembly template were fabricated by curing the polymer in contact with an HSQ master template structure with protruding lines of sub-50 nm width. Upon removing the PDMS from the HSQ template after baking, the HSQ lines are precisely replicated onto PDMS. (b) A SEM image of HSQ lines with a total length of 90  $\mu$ m, a height of  $\sim 60$  nm, and a width of  $38 \pm 2$  nm fabricated on a Si wafer using EBL.

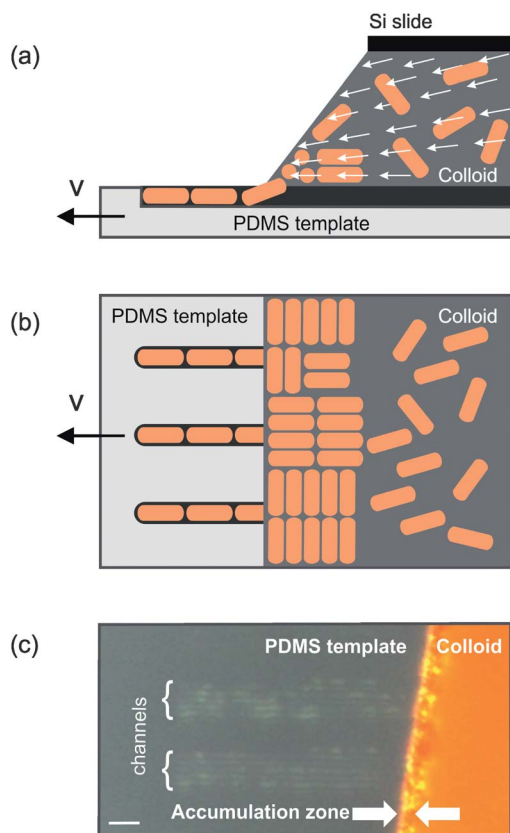


**Fig. 2** Schematic description of the assembly process. (a) A colloidal droplet of Au NRs is deposited onto the polymer template and constrained by the silicon slide. The receding meniscus is moved over the template by moving the stage underneath the PDMS template relative to the slide at constant speed  $v$ . (b) The schematic top view shows that the meniscus is formed perpendicular to the channel structures, with the moving direction parallel to the channels. The Au NRs are thereby deposited into the channels by capillary forces, which direct them from a preferentially perpendicular orientation in the meniscus to an orientation enforced by the channel. (c) An optical microscopy image taken during the assembly shows 90  $\mu\text{m}$  long channels and 60 nm wide channels (each bracket indicates six parallel channels). The bright spots in the channels are the deposited Au NRs. Scale bar is 4  $\mu\text{m}$ .

into 60 nm and 80 nm deep channels was successful. It was not expected that the assembly into 40 nm deep channels would not work as the diameter of the rods was only 24 nm and also as Kuemin *et al.*<sup>38</sup> reported the successful assembly of individual Au NRs with the same dimensions in short  $37 \pm 2$  nm deep linelets (lateral dimensions were  $52 \pm 3$  nm  $\times$   $138 \pm 3$  nm). The fact that for assembly in long lines (compared to Kuemin *et al.*<sup>38</sup>) obviously deeper channels are required indicates that the corresponding assembly mechanism differs from that for short linelets. During the assembly in long channels we can observe that individual Au NRs are released from the meniscus, travel along the channel, and are eventually deposited next to the previously assembled Au NR in the channel. A similar behavior has been observed by Malaquin for the assembly of 500 nm diameter polystyrene particles into lines.<sup>36</sup> Here, we assume that this event is induced by the axial gradient of the capillary pressure in the channel which drives the axial liquid flow. The maximum reach of this effect is then the penetration length of

the fluid drawn into the channel by capillary suction. The penetration length is proportional to the square root of the channel depth<sup>45</sup> and thus deeper channels would facilitate the deposition of the nanorods in this way. If not explicitly mentioned otherwise, all experiments described below were performed with the optimal channel depth of  $60 \pm 3$  nm.

In addition to the template geometry, other process-related parameters also have a strong influence on the assembly experiments. In particular the assembly yield was found to be highly sensitive to changes in the assembly temperature,  $T_{\text{assembly}} = (T_{\text{dew}} + \Delta T)$ ,<sup>39</sup> where  $T_{\text{dew}}$  is the temperature at the dew point. Evaporation of the solvent depends on  $T_{\text{assembly}}$  and promotes a laminar flow within the droplet, which drives the nanorods towards the meniscus where they form a densely packed accumulation zone.<sup>36</sup> We observed that the density of the accumulation zone, which is linked to the assembly temperature, directly influences the assembly yield. To assemble the nanorods into chains requires a constant supply of nanorods at single spots (where the lines are) and therefore

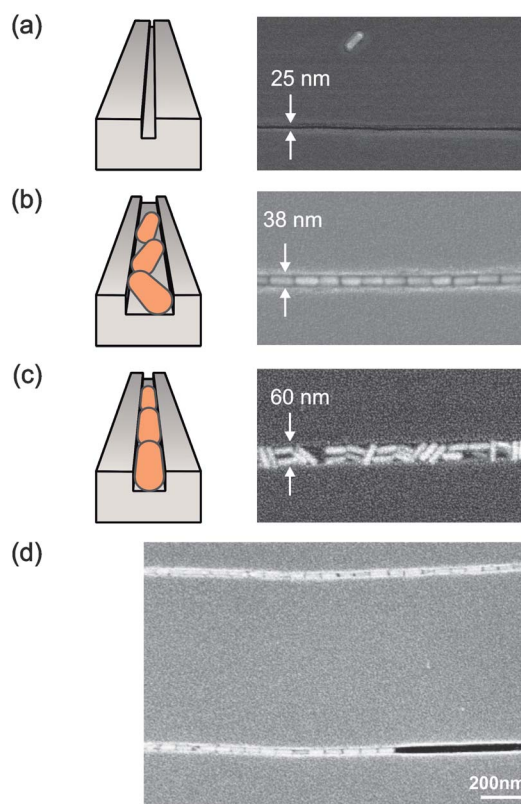


**Fig. 3** Influence of channel width on NR assembly. Three assembly templates with different line widths and their schematics are shown in (a)–(c). After the assembly, about 9 nm of Au was evaporated onto the PDMS templates to enable SEM examination. (a) A channel width of less than 30 nm is too narrow to trap and assemble Au NRs. By chance, a single Au NR did remain on one location after assembly, however all the lines were empty ( $\Delta T = 27$  K). (b) If the channels are more than 50 nm wide, the Au NRs no longer align axially owing to additional rotational degrees of freedom ( $\Delta T = 23$  K). (c) If the channels have the optimal channel width of  $40 \pm 5$  nm, the Au NRs are aligned end-to-end and axially in the channels ( $\Delta T = 27$  K). (d) The assembly process is highly selective and the NRs are deposited only into the channels ( $\Delta T = 27$  K). The apparent bending of the channels is due to charging of the PDMS substrate during SEM imaging.

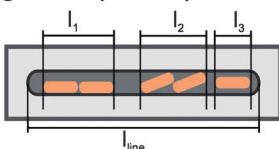
the nanorod supply at these spots defines the length of the chains.

To optimize the yield and the orientation of the Au NRs in the channels towards an end-to-end chain-like formation, a series of assembly experiments was conducted in which the channel width and the assembly temperature  $T_{\text{assembly}}$  were varied (from  $\Delta T = 16$  K to  $\Delta T = 31$  K). For channel widths below 30 nm, not a single Au NR assembled into the channels; in rare cases a rod was found on top of the PDMS surface, to evidence that the meniscus has been moved over the template at all (Fig. 3a). This finding can be explained by the CTAB bilayer that adsorbs on the Au NR surface, thereby forming a layer with a thickness of  $3.2 \pm 0.2$  nm,<sup>46</sup> which increases the apparent Au NR diameter to approx. 30 nm, preventing the Au NRs from assembling into channels of comparable width for simple geometrical reasons. For channels wider than 50 nm, the Au NRs will settle into the channels, but have some remaining degrees of freedom to tilt. Hence, they do not preferentially align strictly along the channel's axis, in the worst case reaching even maximal tilt angles of  $90^\circ$  as shown in Fig. 3b. Our experimental findings yield an optimal channel width of  $40 \pm 5$  nm for a highly deterministic assembly of the Au NRs in two dimensions into an oriented linear chain-like formation (Fig. 3c).

In addition, the assembly experiments were evaluated, both qualitatively and quantitatively. For a quantitative assessment of the assembly, we define the filling factor (FF) given by the section of the channel filled by Au NRs in respect to the entire channel length of  $90 \mu\text{m}$  (Fig. 4a.1). This FF definition disregards details of the orientation or segmented distributions and interruptions of the Au NR chains in the channels. Hence, also a qualitative evaluation is necessary, and we define the following four criteria that need to be fulfilled so that the assembled particles form a *highly deterministic Au NR chain* (Fig. 4a.2). The first criterion (i) is related to the 2D orientational degrees of freedom of the Au NRs within the channel, assuming that they lie flat on the channel bottom. Hereby,  $\theta$  quantifies the misalignment angle of the axis of the assembled Au NRs with respect to the channel axis (Fig. 4a.2.i). Our goal was to reduce any angular degree of freedom that could lead to variations in the inter-particle gap sizes and contact areas. We consider angles of  $|\theta| < \pm 15^\circ$  as tolerable and those chains to be acceptable in terms of criterion (i). The second criterion (ii) is necessary because the colloidal Au NR solution exhibits large variations of particle shapes and sizes (see ESI †). Criterion (ii) thus describes the uniformity of the Au NR chain compositions, which can be disturbed if sphere-like nanoparticles present in the solution are trapped. These small-aspect ratio nanoparticles

### (a) Quantitative and qualitative analysis of the chain

#### 1. Quantitative: Filling Factor (FF in %)

$$FF = \sum l_i / l_{\text{line}}$$


#### 2. Qualitative: Phenomena

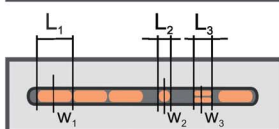
##### i. Orientation

Criterion  $\theta_i < \pm 15^\circ$



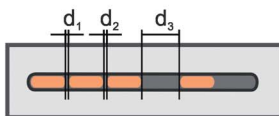
##### ii. Selectivity

Criterion  $L_i/w_i > 1.5$  and  $w_i \approx 20\text{-}30\text{nm}$



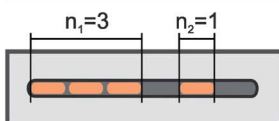
##### iii. Gap Size

Criterion  $d_i \leq 10\text{nm}$



##### iv. Constituents

Criterion  $n_i \geq 3$



### (b) Analysis of the optimal channel width

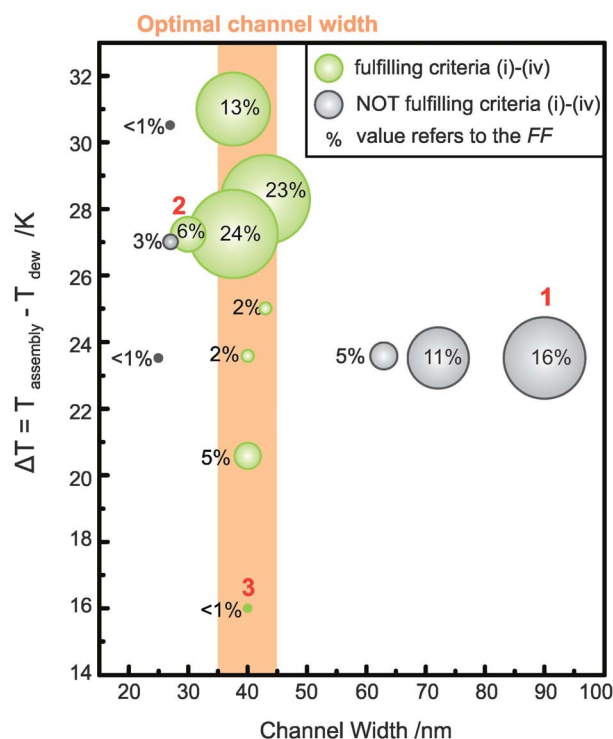


**Fig. 4** (a) Quantitative and qualitative criteria to describe the assembly yield and quality. (b) The evaluation of the assembly experiments is plotted as a function of the temperature ( $\Delta T = T_{\text{droplet}} - T_{\text{dew}}$ ) for different channel widths. Experiments fulfilling criteria (i)–(iv) are represented as green bubbles and non-matching experiments as gray bubbles. The size of the bubble and the percentage value refer to the filling factor FF of the respective assembly experiment. The red numbers in the graph correspond to particular experiments which are discussed in the text. If an experiment was done several times with the same parameters, the results from the experiment with the highest filling factor (FF) were chosen.

can lower the yield of the Au NR chains. We consider the second criterion fulfilled if all particles with length  $L$  and width  $w$  that are aligned in a chain have an aspect ratio of  $L/w > 1.5$  and a width  $w$  in the range of 20–30 nm (Fig. 4a.2.ii). The third criterion (iii) describes the inter-particle distances between the Au NRs as measured using SEM. It is considered fulfilled for gap sizes  $d$  smaller than 10 nm (Fig. 4a.2.iii). The final criterion (iv) considers the overall Au NR chain length defined by the number of Au NRs,  $n$ , constituting a chain. We define that for criterion (iv) to be fulfilled the chain must consist of at least three constituents  $n$  in a row ( $n > 3$ ) (Fig. 4a.2.iv). Consequently, monomers and dimers are not considered to be chains. Only if all four criteria (i)–(iv) are fulfilled, do we consider the assembled Au NRs to indeed form a highly deterministic Au NR chain.

The experimental results of varying the channel width and assembly temperature are summarized in Fig. 4b, which shows the statistical analysis of the assembly performance.

When comparing experiments performed at the same process temperature of  $\Delta T = 23.5$  K, an increasing FF with increasing channel width of the structured template can be observed. Under these conditions, the FF increases from below 1% for 25 nm wide channels to 16% for 90 nm wide channels (point 1 in Fig. 4b). However, only for narrow channel widths of 30–45 nm will all four quality criteria for Au NR chains defined above be fulfilled simultaneously (as illustrated by the green bubbles in Fig. 4b). If considering both the maximum FF and the criteria for the highly deterministic Au NR chains, a channel width in the range of 35–45 nm is determined to be optimal as can be seen from the experiments at point 2 in Fig. 4b at  $\Delta T = 27$  K with FF = 24%. Therefore, we define the *optimal channel width* as that width which fulfills the quality criteria (i)–(iv), yielding the maximum FF (Fig. 4b). For the optimal channel width of  $40 \pm 5$  nm we observe a step-like increase in the FF from FF  $\leq 5\%$  at  $\Delta T < 25$  K (experiment point 3) to FF up to 24% at  $\Delta T > 25$  K.

Next, also the lengths of the individual Au NR chains assembled were examined. Accordingly, we counted the number of chains consisting of a certain number of Au NRs according to criteria (i)–(iv). Fig. 5 shows that short chains of  $n < 10$  are the majority with 80% and that about 20% of the chains consist of more than 10 Au NRs resulting in chain lengths of up to 4  $\mu\text{m}$  (Fig. 5).

### Transfer of the assembled Au NR chains

The Au NRs trapped in the assembly template channels can be transferred onto a Si/SiO<sub>2</sub> substrate by micro-contact printing.<sup>37</sup> By using the assembly templates with the trapped Au NR chains as stamp the Au NR chains were transferred from the template onto the target substrate. The target substrate was typically a highly doped piece of p-type Si wafer with a 30 nm layer of SiO<sub>2</sub> covered with a 50 nm thick polymethylmethacrylate (1% PMMA in anisole) layer. The PMMA serves as an adhesion layer for transferring the Au NRs. Our experiments show that the depth of the assembly channels is crucial for the yield of transfer because of the competing adhesion forces of the substrate–NR interface and the PDMS-channel–NR interfaces. The Au NRs

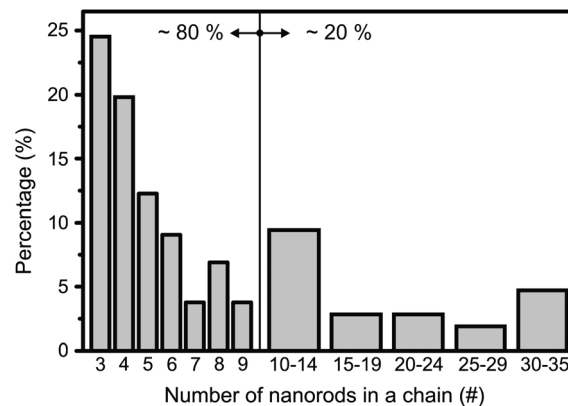


**Fig. 5** The histogram depicts the analysis of three assembly experiments with  $\Delta T_1 = 27$  K,  $w_1 = 38$  nm,  $\Delta T_2 = 28$  K,  $w_2 = 43$  nm,  $\Delta T_3 = 31$  K,  $w_3 = 38$  nm and a channel depth of  $60 \pm 3$  nm for all three experiments. First, the Au NRs in the individual chains were counted. Then the number of chains with a particular number of Au NRs is given in percentage of their appearance in the channels of the nanostructured template. Only those Au NRs that were compliant with all four quality criteria (i)–(iv) were counted.

that had been assembled into the  $80 \pm 3$  nm deep channels could not be released from the polymer template by this printing method, because they are too deeply trapped in the channel. In contrast, the method performs well for channels with  $60 \pm 3$  nm depth. Fig. 6a shows the Au NR chains embedded in PMMA after the transfer from the 60 nm deep channels. Because the Au NRs need to be in intimate contact with the target substrate for further processing, the PMMA adhesion layer was removed subsequent to the transfer by exposing the substrates to oxygen plasma (see also ESI 2†). The substrates were finally rinsed in acetone and isopropanol and dried with N<sub>2</sub>. As demonstrated in Fig. 6b, the chain-like formation of the Au NRs could be preserved. For the resulting Au NR chains, the inter-particle distances were measured by SEM to be in the range of 5–7 nm (Fig. 6c), not altered by the oxygen plasma treatment within the experimental resolution available for gap-size measurements.

The gap sizes are considered plausible taking into account a CTAB bilayer of  $\sim 3.2$  nm thickness on the Au NR surface, which would correspond to gaps of approx. 6 nm when disregarding interlayer interdigitation. This estimation is in good agreement with our experimental findings, and we conclude therefore that the gap between the Au NRs is defined primarily by the thickness of the CTAB bilayer acting as the spacer rather than any other assembly parameters.

### Electrical characterization of the Au NR chains

The target substrates were pre-patterned with large Au contact pads to enable electrical contacting of the sample in a needle probe setup. The printed Au NR chains were wired to the contact pads by EBL, metallization and lift-off technique. This was done by first mapping the Au NR chains in respect to predefined markers on the target substrates using SEM. A PMMA resist (4% in anisole) was spin-coated onto the substrate and selectively structured by EBL. After the development of the resist, a layer of

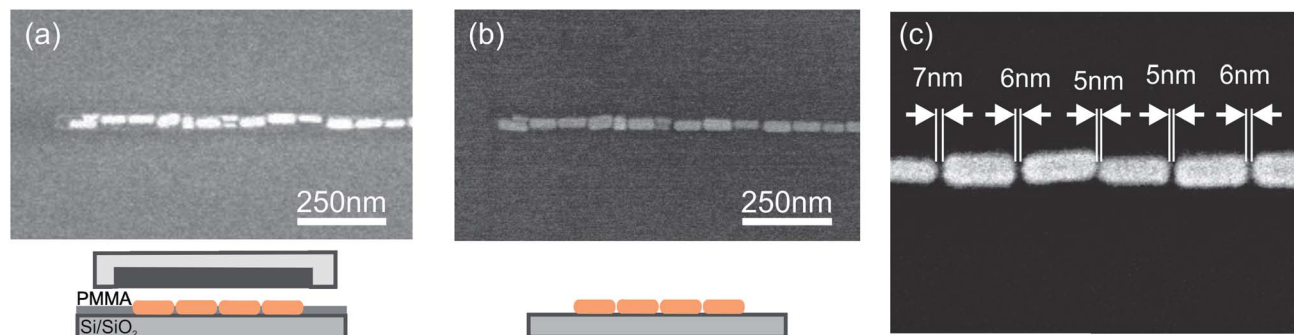


**Fig. 6** (a) An Au NR chain printed on a Si/SiO<sub>2</sub> substrate using an ~50 nm thick PMMA adhesion layer. (b) The PMMA was etched away by oxygen plasma. After additional cleaning of the samples with acetone and isopropanol, the Au NRs preserve their original position. (c) The interparticle distances between the Au NRs were measured by SEM to be between 5 and 7 nm.

5 nm titanium (Ti) and 50 nm Au was evaporated onto the sample and a lift-off step removed the excess material and revealed the desired electrode structures. To remove possible contamination that may have been trapped during the various processing steps, the samples were cleaned in fuming nitric acid for 1 min, then rinsed in water and dried with N<sub>2</sub>. The resulting devices comprise a linear 1D Au NR chain with nanometer-sized junctions wired to Au leads. Au NR chain devices prepared in this way were electrically characterized under vacuum at ambient temperature (293 K). As an example, a sample consisting of three Au NR chains contacted in parallel is shown in Fig. 7a. Fig. 7b shows the corresponding *I*-*V* characteristics of the three parallel chains with 12 gaps for each line, measured in a voltage range of -10 V to +10 V. The current is found to fluctuate between ±1 pA, indicating the noise level of the setup (Fig. 7b, gray curve). The low conductance indicates that no conductive percolation path by possible melting of the Au NR chain has been created during the contact fabrication process and that the nanogaps are still present.

With their metallic characteristic and restricted tip surface area (<1 μm<sup>2</sup>), the Au NR chains are ideal as electrodes for molecular charge transport measurements. In the next step, we therefore integrated functional organic molecules into the Au NR chains as a first demonstration of the Au NR platform for nano-electronic applications. The sample was immersed for 48 h into a 1 mM solution with thiol end-capped OPV-5 molecules dissolved in tetrahydrofuran (THF). The OPV-5 molecule was chosen because of its relatively high electrical conductance (Fig. SI 3† shows the molecular structure of the OPV-5).<sup>47</sup> Directly after OPV-5 immersion, the Au NR chain device was characterized under vacuum at room temperature (293 K). A significantly higher current flow (Fig. 7b, red curve) than in the measurement of the same device prior to functionalization was observed. At an applied voltage of 10 V, a current of 1 nA is detected, which is three orders of magnitude higher than the value measured (limited by the noise level) prior to immersion in the OPV-5 solution as shown in the inset of Fig. 7b. The OPV-5 molecule has five benzene rings connected through four double bonds, resulting in a total length of 3.2 nm. Thus the molecule is too short to directly bridge the gaps of ~6 nm between the individual Au NRs. Our measurements indicate that the

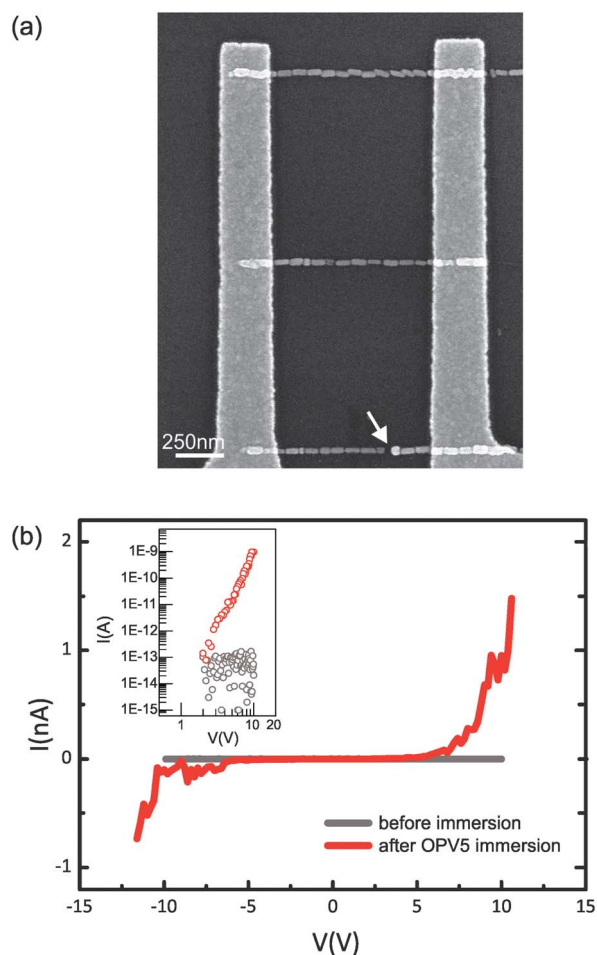


**Fig. 7** (a) Three Au NR chains were contacted in parallel. The white arrow indicates a nanoparticle that does not meet criterion (ii) for highly deterministic Au NR chains and disrupts the chain formation. Owing to the very large gap, this line is nominally deactivated for electrical characterization. (b) The *I*-*V* characteristics were measured before (grey curve) and after immersion in OPV-5 molecules (red curve). The inset shows the double logarithmic representation log(*I*)-log(*V*) in the range of 2 to 10 V.

molecular building blocks significantly increase the conductivity of the nanogap and promote tunneling currents across the Au NR chain by molecular-mediated transport. In gaps less than

6 nm, an aromatic  $\pi$ - $\pi$  coupling between adjacent molecules would be possible, which was shown to be sufficiently efficient to allow for the controlled formation of molecular bridges between electrodes.<sup>48,49</sup>

### 3 Conclusions

In summary, this study demonstrated the well-controlled and reproducible assembly of linear gold nanorod chains up to 4  $\mu\text{m}$  in length with a gap size of about 6 nm and their transfer to a generic silicon substrate. The gap size was found to be well defined by the protecting surfactant CTAB bilayer. It is assumed that by exchanging the CTAB bilayer on the Au NRs with another surfactant in solution, the gap between the Au NRs for the assembly can be tailored to a large extent. This would allow the fabrication of tailored Au NR chains of various lengths for molecular building blocks or with variable gap sizes for optical or plasmonic applications. We show that the parameter window for successful assembly of the anisotropic gold nanorods into strictly linear chains is very narrow and the critical parameters were identified to be the channel width and depth (in respect to a given nanoparticle size), and the assembly temperature. These parameters were studied and found to be optimal with  $40 \pm 5$  nm for the width,  $60 \pm 3$  nm for the depth, and  $\Delta T \geq 25$  K for the assembly temperature (note that the upper  $\Delta T$  is limited by pinning effects; experiments with  $\Delta T$  up to 31 K were performed) in the specific case of Au NRs with  $\sim 64$  nm length and  $\sim 24$  nm width. The precise alignment shows the high impact and versatility of the capillary assembly technique, which enables very accurate deposition of highly anisotropic nanoparticles if the appropriate parameters are used. At this high level of assembly, the main limiting factor for the experiments is the non-homogeneous size of the Au NRs, which was found to have a determinant influence on the assembly.

Furthermore, the Au NR chains were electrically contacted and measurements could be performed on samples prior to and after immersion into a solution of OPV-5 molecules. After immersion, the conductance increased by three orders of magnitude at 10 V, adducing evidence for molecule-mediated transport. The platform is thus ideally suited to serve as a test bed for long molecular wires. Moreover, optical experiments investigating strong field enhancements due to concentration of plasmonic modes are currently ongoing.

Therefore, the established method serves as an excellent platform to fabricate structures for applications in nano-electronics and nano-optics.

## 4 Experimental section

### Template fabrication process

Assembly templates were produced by molding liquid poly(dimethylsiloxane) (PDMS) against a Si master comprising fin-like nanostructures (see Fig. 1a). The fins are fabricated by spin-coating the negative resist hydrogen silsesquioxane (HSQ, see Table SI 4†) on a Si wafer and exposing thin lines by EBL (aperture 10  $\mu\text{m}$ , 20 kV, line dose was varied depending on line

thickness). After exposure, the HSQ was developed in sodium hydroxide (1%) for 90 s and annealed at 400  $^{\circ}\text{C}$  for 1 h. These fin-like HSQ-structures can be reused several times as the master for molding the PDMS templates.

For the replica-molding process the PDMS was squeezed between the wafer master and a glass backplane. The latter was exposed to vinyltrichlorosilane (97%, ABCR, Karlsruhe, Germany) in a desiccator (2 min, 200 mbar) to promote the adhesion to PDMS. To enable easy removal of the PDMS from the wafer templates, the Si was coated with 1H,1H,2H,2H-perfluorodecyltrichlorosilane from the gas phase in a desiccator (2 min, 25 mbar), followed by thermal annealing (60  $^{\circ}\text{C}$ , 50 mbar, 1 h). Molds were cured (48 h, 60  $^{\circ}\text{C}$ ) before the PDMS together with the supporting glass backplane were detached from the silicon master. The templates were then rinsed in ethanol for 24 h to extract low-molecular-weight silicone oils and dried for 30 min at 20 mbar at room temperature.

### Preparation of the Au NR suspension

The Au NRs that are stabilized in a cetyltrimethylammonium-bromide (CTAB) solution (Nanopartz Inc., USA) have an aspect ratio of 3.2 and a surface plasmon resonance (SPR) peak at 729 nm. By centrifuging, decanting, and adding CTAB, the free CTAB concentration in the solution was adjusted to 0.9 mM, in accordance with the critical micelle concentration (cmc).<sup>50</sup> At concentrations lower than the cmc, the colloidal solution is not stable and the gold nanorods tend to agglomerate during the assembly. The Au NR suspension was filtered using Millex-LG, 0.2  $\mu\text{m}$ , hydrophilic PTFE pore filters (Millipore, Zug, Switzerland) and was centrifuged again to adjust the concentration of the Au NRs to  $\text{cNR} = 10^{12}$  nps per mL. A droplet of  $\sim 50$ –60  $\mu\text{L}$  of the suspension was used for each assembly experiment.

### Capillary assembly experiments

The capillary assembly experiments were conducted in a setup described earlier.<sup>39</sup> Briefly, the home-built setup enables control of the speed of the moving meniscus as well as of the temperature of the Au NR suspension during the assembly. The PDMS templates were fixed onto a Peltier element, which itself sits on a linear translational stage. A droplet of the Au NR colloid solution was injected between the assembly template and a stationary mounted silicon slide (size  $\sim (1 \times 10)$   $\text{cm}^2$ ) at a distance of  $\sim 2$  mm above the PDMS template. Prior to their use, the silicon slides were rendered hydrophobic by adsorbing dodecyltrichlorosilane (97%, ABCR, Karlsruhe, Germany) from the gas phase in a desiccator (10 min, 200 mbar). The speed for all experiments was set to 0.1  $\mu\text{m s}^{-1}$ . The meniscus forms an angle of  $50 \pm 10^{\circ}$  with the PDMS template, slightly varying during the assembly. To account for possible variations in the humidity (varying in the range of 30% to 60%) and ambient temperature, the assembly temperatures were adjusted relative to the dew point,  $T_{\text{dew}}$ . If an experiment was done several times with the same parameters, the results from the experiment with the highest filling factor (FF) were chosen for the table in Fig. 4b.

### Au NR transfer method

The transfer of the Au NRs from the PDMS assembly template onto the target Si/SiO<sub>2</sub> substrate by micro-contact printing was done using a home-built tool. A droplet (10 μL) of poly(methyl methacrylate) (PMMA, 1% in anisole, 950k) was sandwiched between the assembly template and the target substrate by applying a force of ~50 N and subsequently heated up to 130 °C for 10 min. After cooling the setup down to room temperature, the assembly template was released and the Au NRs were transferred onto the target substrate, embedded into the PMMA layer. The approximately 50 nm thick PMMA layer was removed by several oxygen plasma cycles with pauses of ~60 s in between to avoid heating. The NR chains were examined by SEM imaging and the inter-particle distances were measured to be ~6 nm. The measurements are restricted in precision related to the resolution limit of the SEM (Hitachi, SU8000) which is in the order of ~1.5 nm at 10 kV.

### Preparation of Au NR chain samples for measurements

Highly doped (p-type, 0.002–0.003 Ω cm) Si wafers with a 30 nm thin thermal SiO<sub>2</sub> layer were used as target substrates. Metal pads comprising 10 nm Ti/80 nm Au and having a size of (250 × 250) μm<sup>2</sup> were patterned using UV photolithography and lift-off technique. To connect the nanorods with the prefabricated metal pads, EBL was performed with a Raith e-line tool. PMMA (4% in anisole, 950k) was spin-coated onto the target substrate (4000 rpm, 40 seconds), cured on a hot plate (185 °C, 90 seconds), and then exposed (10 μm aperture, 10 kV, 180 μC cm<sup>-2</sup> area dose). The resist was developed in an isopropanol-water mixture (IPA-H<sub>2</sub>O = 3 : 1) for 50 s in an ultrasonic bath. A 5 nm Ti/50 nm Au layer was evaporated, and lift-off was done in acetone, followed by isopropanol rinsing and nitrogen drying. Immersion of the sample in the molecule solution was done under argon atmosphere for 48 h. The electrical characterization was performed in a four-probe setup under vacuum (5 × 10<sup>-2</sup> mbar) using an Agilent Semiconductor device analyzer B1500A.

### Chemical synthesis of molecules

The (*E,E*)-1,4-bis[4-((*E*)-4-(acetylthio)styryl)styryl]-2,5-didodecylbenzene (OPV-5 Ac) molecule was synthesized according to known synthetic procedures.<sup>51</sup> In brief, the molecule was synthesized *via* Wittig-type reactions. The thiols were protected as their *tert*-butyl thioethers throughout the reaction sequence and converted into labile acetyl-protected thiols in the last reaction step. Boiling the OPV-5 Ac in toluene containing trace amounts of iodine yielded the all-*trans* compound as pale-yellow crystals.

### Acknowledgements

The work was supported by the European Community Seventh Framework Program (FP7/2007-2013) under the Grant Agreement No. 213609 "SINGLE". The authors thank H. Schmid for support in SEM imaging, V. Schmidt, B. Gotsmann, C. Kuemin and M. Klein for discussions, M. Tschudy, U. Drechsler,

D. Caimi and R. Beyeler for their technical contributions, and W. Riess for continuous support.

### Notes and references

- 1 A. Zabet-Khosousi and A.-A. Dhirani, *Chem. Rev.*, 2008, **108**, 4072.
- 2 J. M. Wessels, H. G. Nothofer, W. E. Ford, F. von Wrochem, F. Scholz, T. Vossmeier, A. Schroedter, H. Weller and A. Yasuda, *J. Am. Chem. Soc.*, 2004, **126**, 3349.
- 3 C. P. Husband, S. M. Husband, J. S. Daniels and J. M. Tour, *IEEE Trans. Electron Devices*, 2003, **50**, 1865.
- 4 J. Liao, L. Bernard, M. Langer, C. Schönenberger and M. Calame, *Adv. Mater.*, 2006, **18**, 2444.
- 5 L. Bernard, Y. Kamdzhilov, M. Calame, S. J. van der Molen, J. Liao and C. Schönenberger, *J. Phys. Chem. C*, 2007, **111**, 18445.
- 6 K. Matsuda, H. Yamaguchi, T. Sakano, M. Ikeda, N. Tanifuji and M. Irie, *J. Phys. Chem. C*, 2008, **112**, 17005.
- 7 S. J. van der Molen, J. Liao, T. Kudernac, J. S. Adustsson, L. Bernard, M. Calame, B. J. van Wees, B. L. Feringa and C. Schönenberger, *Nano Lett.*, 2009, **9**, 76.
- 8 D. Conklin, S. Nanayakkara, T. H. Park, M. F. Lagadec, J. T. Stecher, M. J. Therien and D. A. Bonnell, *Nano Lett.*, 2012, **12**, 2414.
- 9 M. Li, R. B. Bhiladvala, T. J. Morrow, J. A. Sloss, K.-K. Lew, J. M. Redwing, C. D. Keating and T. S. Mayer, *Nat. Nanotechnol.*, 2008, **3**, 88.
- 10 H. Nakanishi, D. A. Walker, K. J. M. Bishop, P. J. Wesson, Y. Yan, S. Soh, S. Swaminathan and B. A. Grzybowski, *Nat. Nanotechnol.*, 2011, **6**, 740.
- 11 P. K. Jain, X. Huang, I. H. El-Sayed and M. A. El-Sayed, *Acc. Chem. Res.*, 2008, **41**, 1578.
- 12 S. Eustis and M. A. El-Sayed, *Chem. Soc. Rev.*, 2006, **35**, 209.
- 13 H. A. Atwater and A. Polman, *Nat. Mater.*, 2010, **9**, 205.
- 14 P. Banerjee, D. Conklin, S. Nanayakkara, T. H. Park, M. J. Therien and D. A. Bonnell, *ACS Nano*, 2010, **4**, 1019.
- 15 K. J. M. Bishop, C. E. Wilmer, S. Soh and B. A. Grzybowski, *Small*, 2009, **5**, 1600.
- 16 M. Grzelczak, J. Vermant, E. M. Furst and L. M. Liz-Marzán, *ACS Nano*, 2010, **4**, 3591.
- 17 Z. Nie, A. Petukhova and E. Kumacheva, *Nat. Nanotechnol.*, 2010, **5**, 15.
- 18 X. Huang, S. Neretina and M. A. El-Sayed, *Adv. Mater.*, 2009, **21**, 4880.
- 19 E. C. Dreaden, A. M. Alkilany, X. Huang, C. J. Murphy and M. A. El-Sayed, *Chem. Soc. Rev.*, 2012, **41**, 2740.
- 20 C. J. Murphy, L. B. Thompson, A. M. Alkilany, P. N. Sisco, S. P. Boulos, S. T. Sivapalan, J. A. Yang, D. J. Chernak and J. Huang, *J. Phys. Chem. Lett.*, 2010, **1**, 2867.
- 21 L. Vigderman, B. P. Khanal and E. R. Zubarev, *Adv. Mater.*, 2012, **24**, 4811.
- 22 K. Liu, N. Zhao and E. Kumacheva, *Chem. Soc. Rev.*, 2011, **40**, 656.
- 23 Z. Liu, H. Huang and T. He, *Small*, 2013, **9**, 505.
- 24 D. Nepal, M. S. Onses, K. Park, M. Jespersen, C. J. Thode, P. F. Nealey and R. A. Vaia, *ACS Nano*, 2012, **6**, 5693.

- 25 K. G. Thomas, S. Barazzouk, B. I. Ipe, S. T. S. Joseph and P. V. Kamat, *J. Phys. Chem. B*, 2004, **108**, 13066.
- 26 K. K. Caswell, J. M. Wilson, U. H. F. Bunz and C. J. Murphy, *J. Am. Chem. Soc.*, 2003, **125**, 13914.
- 27 Z. Nie, D. Fava, E. Kumacheva, S. Zou, G. C. Walker and M. Rubinstein, *Nat. Mater.*, 2007, **6**, 609.
- 28 Z. Nie, D. Fava, M. Rubinstein and E. Kumacheva, *J. Am. Chem. Soc.*, 2008, **130**, 3683.
- 29 T. S. Sreepasad, A. K. Samal and T. Pradeep, *Langmuir*, 2008, **24**, 4589.
- 30 A. Petukhova, J. Greener, K. Liu, D. Nykypanchuk, R. Nicolaÿ, K. Matyjaszewski and E. Kumacheva, *Small*, 2012, **8**, 731.
- 31 H. Häkkinen, *Nat. Chem.*, 2012, **4**, 443.
- 32 T. Jain, S. Lara-Avila, Y.-V. Kervennic, K. Moth-Poulson, K. Nørgaard, S. Kubatkin and T. Bjørnholm, *ACS Nano*, 2012, **6**, 3861.
- 33 Y. Yin, Y. Lu, B. Gates and Y. Xia, *J. Am. Chem. Soc.*, 2001, **123**, 8718.
- 34 Y. Xia, Y. Yin, Y. Lu and J. McLellan, *Adv. Funct. Mater.*, 2003, **13**, 907.
- 35 X. Xiong, P. Makaram, A. Busnaina, K. Bakhtari, S. Somu, N. McGruer and J. Park, *Appl. Phys. Lett.*, 2006, **89**, 193108.
- 36 L. Malaquin, T. Kraus, H. Schmid, E. Delamarche and H. Wolf, *Langmuir*, 2007, **23**, 11513.
- 37 T. Kraus, L. Malaquin, H. Schmid, W. Riess, N. D. Spencer and H. Wolf, *Nat. Nanotechnol.*, 2007, **2**, 570.
- 38 C. Kuemin, L. Nowack, L. Bozano, N. D. Spencer and H. Wolf, *Adv. Funct. Mater.*, 2012, **22**, 702.
- 39 C. Kuemin, R. Stutz, N. D. Spencer and H. Wolf, *Langmuir*, 2011, **27**, 6305.
- 40 F. Holzner, C. Kuemin, P. Paul, J. L. Hedrick, H. Wolf, N. D. Spencer, U. Duerig and A. W. Knoll, *Nano Lett.*, 2011, **11**, 3957.
- 41 J. Pérez-Juste, I. Pastoriza-Santos, L. M. Liz-Marzán and P. Mulvaney, *Coord. Chem. Rev.*, 2005, **249**, 1870.
- 42 C. Sönnichsen and A. P. Alivisatos, *Nano Lett.*, 2005, **5**, 301.
- 43 C. J. Orendorff, T. M. Alam, D. Y. Sasaki, B. C. Bunker and J. A. Voigt, *ACS Nano*, 2009, **3**, 971.
- 44 M. Geissler, H. Wolf, R. Stutz, E. Delamarche, U. W. Grummt, B. Michel and A. Bietsch, *Langmuir*, 2003, **19**, 6301.
- 45 R. H. Nilson, S. W. Tchikanda, S. K. Griffiths and M. J. Martinez, *Int. J. Heat Mass Transfer*, 2006, **49**, 1603.
- 46 S. Gómez-Graña, F. Hubert, F. Testard, A. Guerrero-Martínez, I. Grillo, L. M. Liz-Marzán and O. Spalla, *Langmuir*, 2012, **28**, 1453.
- 47 S. Kubatkin, A. Danilov, M. Hjort, J. Cornil, J.-L. Brédas, N. Stuhr-Hansen, P. Hedegård and T. Bjørnholm, *Nature*, 2003, **425**, 698.
- 48 S. Wu, M. T. González, R. Huber, S. Grunder, M. Mayor, C. Schönenberger and M. Calame, *Nat. Nanotechnol.*, 2008, **3**, 569.
- 49 T. Hassenkam, K. Moth-Poulson, N. Stuhr-Hansen, K. Nørgaard, M. S. Kabir and T. Bjørnholm, *Nano Lett.*, 2004, **4**, 19.
- 50 S. P. Moulik, M. E. Haque, P. K. Jana and A. R. Das, *J. Phys. Chem.*, 1996, **100**, 701.
- 51 N. Stuhr-Hansen, J. B. Christensen, N. Harrit and T. Bjørnholm, *J. Org. Chem.*, 2003, **68**, 1275.